Extreme Wave Run-up and Pressure on a Vertical Seawall

Dezhi Ning[a], Rongquan Wang[a], Lifen Chen[a,*], Jinxuan Li[a], Jun Zang[a, b], Liang Cheng[a, c] , Shuxue Liu[a]

[a]State Key Laboratory of Coastal and offshore Engineering, Dalian University of Technology, Dalian, 116024, China.
[b]Department of Civil and Architecture Engineering, University of Bath, Bath, BA2 7AY, UK.
[c]School of Civil, Environmental and Mining Engineering, University of Western Australia, Crawley, WA 6009, Australia

ABSTRACT:

The performance of coastal vertical seawalls in extreme weather events is studied numerically, aiming to provide guidance in designing and reassessing coastal structures with vertical wall. The extreme wave run-up and the pressure on the vertical seawall are investigated extensively. A time-domain higher-order boundary element method (HOBEM) is coupled with a mixed Eulerian-Lagrangian technique as a time marching technique. Focused wave groups are generated by a piston wave-maker in the numerical wave tank using a wave focusing technique for accurately reproducing extreme sea states. An acceleration-potential scheme is used to calculate the transient wave loads. Comparisons with experimental data show that the extended numerical model is able to accurately predict extreme wave run-ups and pressures on a vertical seawall. The effects of the wave spectrum bandwidth, the wall position and the wave nonlinearity on the wave run-up and the maximum wave load on the vertical seawall are investigated by doing parametric studies.

Keywords: Extreme sea states; Wave pressure; Wave run-up; Fully nonlinear potential flow theory; Coastal vertical seawall.

1. INTRODUCTION

Extreme waves, which are also known as freak waves, rogue waves or killer waves, are relatively large and rare local water surface elevations that pose potential threats even to navigation vessels and offshore structures. The occurrence of extreme waves has been well documented and is believed to be responsible for many reported accidents. A list of eleven documented catastrophic ship collisions off the Indian Coast of South Africa was reported as a result of freak waves [1]. Lavrenov [2] found that the mechanism of

*Corresponding author.
E-mail addresses: dzning@dlut.edu.cn (D.Z. Ning), 565196623@qq.com (R.Q. Wang),chenlifen239@163.com (L.F. Chen),jxli@dlut.edu.cn (J.X. Li), jz235@bath.ac.uk (J. Zang), liang.cheng@uwa.edu.au (L. Cheng), sxliu@dlut.edu.cn (S.X. Liu)

wave concentration due to Agulhas counter-current may explain the formation of these freak waves. Sand et al. [3] identified several freak waves on the Danish Continental Shelf, which were found to be responsible for the platform damage at the Ekofish field in the Norwegian Sector of the North Sea. Observations of freak waves in many areas of the World Ocean suggest that freak waves not only exist in offshore deep water but also occur in coastal zones. Freak wave phenomena on-shore, which result in sudden unexpected flooding of coastal areas and strong impacts on coastal structures, were described in [4, 5]. There were 140 freak wave events being observed in the coastal zone of Taiwan from 1949 to 1999 [6]. It was found that six out of nine freak wave events in 2005 occurred nearshore [7].

Extreme conditions must be considered in the design of coastal structures to ensure safety and stability of these structures, given that over 80% of reported past freak wave events occurred in shallow waters or coastal areas [3, 8, 9]. Vertical wall-type structures have been widely adopted as the coastal protection structures, with the advantages that they are able to reflect incidental wave energy almost completely and provide a calm zone for safe berthing of vessels. Additionally, it is found that the sloping walls lead to an increase in the run-up by up to 55% [10] and experience larger wave loading and pressures [11] when compared to those for the vertical seawalls. Thus, accurate prediction of the extreme wave loading on vertical seawalls is important and forms a focus of this study.

In the existing design methods, extreme waves are usually simulated by periodic waves with the wave height and the wave period corresponding to identified extreme conditions. Extensive research has been carried out for investigating pressures on vertical walls due to regular waves, such as [12 - 14]. The Goda formula [12] is one of the most popular equations for the design of coastal structures, and has been adopted by Japan Standard for estimating wave forces on vertical walls [37]. Lin [15] carried out a series of experiments to measure pressures on vertical breakwaters in the presence of regular waves and found that the pressure distributions on vertical walls are different from those predicted by Goda's theory.

The random and broad-banded nature of ocean waves cannot be taken into account by using regular waves. This often leads to inaccuracy in the estimation of fluid loading for practical applications. The experimental study in [16] shown that the maximum pressure on the vertical wall due to irregular waves is larger than that in regular waves near the still water level. Chiu et al. [17] found that the use of regular wave leads to an underestimation of wave forces acting on vertical breakwaters by comparing the results of regular waves and irregular waves. They found that the Goda formula [12] would either under-estimate or over-estimate the wave forces on the vertical wall. More studies on random wave impacting on vertical walls can be found in [18 - 20].

Random wave simulation is very inefficient due to requirements of very long run-time in order to capture near-extreme events. Wave reflection due to finite sized tanks is another issue in long time-domain simulations. An accurate description of the average shape of an extreme event, in which a single large event formed by focusing all wave components tapers away either side of the large crest, provides a good alternative to random waves. This type of extreme events is commonly referred to as a focused wave group in which both the frequency spectrum and phase of the wave components are carefully controlled so that the constructive interference occurs at one point in space and time. Tromans et al. [21] proposed a design formulation to describe the mean shape of an extreme event, and this formulation has subsequently been validated by comparing with field measurements in [22]. Baldock et al. [23] presented a series of physical experiments in which a large transient wave group was produced by focusing a large number of wave components. The focused wave group technique has also been used for studying extreme events from a given random sea-state of known spectral content [24 - 31].

To date, the knowledge on wave pressures due to focused wave groups on vertical seawalls is still rather limited. Improved understanding of spectral and extreme characteristics of wave pressure on a vertical seawall has the potential to lead to better and safe designs of coastal and offshore structures. In this paper, the fully nonlinear numerical model developed to study the evolution of the focused wave group in [32] is extended in this research. The present work is focused on the assessment of how the extended fully nonlinear numerical model performs when applied to investigate extreme wave loading on a vertical seawall. The model solved the Laplace equation for describing the fluid motion based on the time-domain higher-order boundary element method (HOBEM). A new input boundary condition is proposed to generate focused wave groups by imitating wave paddles in real wave tanks. The numerical results are compared with published experimental data, and favorable agreements are achieved. The variations of wave pressure along the wall height are presented and the effect of wave spectra on the wave pressure distribution is subsequently investigated.

2. Numerical method

The concerned problem can be described as an initial-boundary value problem mathematically and solved by a time-domain higher-order boundary element method (HOBEM) in which a mixed Eulerian-Lagrangian technique and a 4th - order Runge-Kuatta scheme are applied as a time marching technique [32]. The present model is an extension to the model developed in [32] where a fully nonlinear solution of Laplace equation was obtained with a set of addition constraints for describing the evolution and wave

kinematic of focused wave groups. In the present model, new boundary conditions are added to extend the capacity of the numerical model in [32] in simulating the interaction between focused wave groups and vertical seawalls. The underlying equation and algorithm are summarized in this section.

2.1. Governing equation and boundary conditions

The simplified geometry of an extreme wave hitting on a vertical seawall is shown in Fig.1. A Cartesian coordinate system *Oxz* is introduced such that the origin *O* is in the plane of the undisturbed free surface, $x = 0$ at the left end of the domain, z positive upwards. It is assumed that the fluid is incompressible, inviscid and the flow irrotational so that a velocity potential $\phi(x, z, t)$ exists and satisfies the Laplace equation inside the fluid domain Ω,

$$\nabla^2\phi = 0 \text{ , in } \Omega \tag{1}$$

The fluid domain Ω is bounded by the instantaneous free surface Γ_{f}, the flume bottom Γ_{d} and the vertical end-wall Γ_{r} as well as the input boundary Γ_{I} on which additional constraints are posed to ensure a unique solution. That is, both the fully nonlinear kinematic and dynamic boundary conditions are satisfied on Γ_{f}, and on both Γ_{d} and Γ_{r}, the rigid and impermeable boundary condition is satisfied,

$$\begin{cases} \dfrac{Dx_s}{Dt} = \nabla\phi, \dfrac{D\phi}{Dt} = -g\eta + \dfrac{1}{2}\nabla\phi\cdot\nabla\phi, \text{ on } \Gamma_{\mathrm{f}} \\ \dfrac{\partial\phi}{\partial n} = 0, \text{ on } \Gamma_{\mathrm{d}} \text{ and } \Gamma_{\mathrm{r}} \end{cases} \tag{2}$$

where g represents the acceleration due to gravity, x_s denotes the position vector of a fluid particle on the free surface, η is the instantaneous free surface elevation and D/Dt is the material derivative.

Additionally, rather than [32] in which focused wave groups were generated by specifying the velocities on the inlet boundary based on experimental measurements, incident waves here are generated by a piston-type wave-maker in which the motion of the wave-maker S and its velocity u_p are prescribed on Γ_{I}.

$$\begin{cases} S = S_a \sin\omega t \\ u_p = S_a \cos\omega t \end{cases}, \quad \begin{cases} S = \sum_{i=1}^{N} S_{a,i} \sin(k_i x_p + \omega_i (t - t_p)) \\ u_p = \sum_{i=1}^{N} S_{a,i}\omega_i \cos(k_i x_p + \omega_i (t - t_p)) \end{cases} \text{ on } \Gamma_{\mathrm{I}} \tag{3}$$

The first of these expressions is for regular waves, the second is for focused wave groups, where s_a and ω are the stroke and the angular frequency of the wave-maker, respectively. For focused wave groups, N is the total number of wave components, k_i and ω_i are the wave number and the angular frequency of the ith wave component satisfying the dispersion relation $\omega_i^2 = gk_i \tanh k_i h$. x_p and t_p denote the focal position and the focal time, respectively.

The relationship between the linear wave amplitude a_i and the wave-maker stroke $S_{a,i}$ can be determined as follows assuming linear focus behavior from the wave paddle [33],

$$S_{a,i} = a_i / Tr \tag{4}$$

where $Tr = 4\sinh^2(k_i h)/(2k_i h + \sinh(2k_i h))$ is the transfer function for piston-type wave-maker and h is the static water depth.

A ramping function is applied to increase the motion of the wave-maker gradually,

$$R_m = \begin{cases} \frac{1}{2}(1-\cos(\frac{\pi t}{T_m})) & \text{if } t \le T_m \\ 1 & \text{if } t > T_m \end{cases} \tag{5}$$

where T_m is a short time duration during which the input wave is ramped. In this study, for regular waves $T_m = 2T$, and $T_m = 2T_{max}$ for focused wave groups in which T_{max} is the largest wave period of wave components.

As the above boundary value problem is solved in the time domain, the calm initial water surface conditions are applied in this research.

2.2. Solver and algorithm

Generally, the aforementioned governing equation together with a set of boundary conditions can be transformed to a boundary integral equation by using second Green's theorem. Then the initial-boundary value problem is solved with the HOBEM by arranging Rankine sources on all surfaces. The 4th - order Runge-Kutta (RK4) scheme is applied to advance the boundary condition on the free surface in Eq. (2) in time. Because of the motion of wave maker, the fluid domain is re-meshed at each time step to avoid unrealistically large mesh deformation. Based on the horizontal coordinates of new nodes obtained from the re-meshing process, the vertical position and the potential can be calculated by interpolation using the quadratic shape function. The detail of the fully nonlinear wave flume used in this study can be found in [32].

146 2.3. Wave pressure on the vertical wall

147 After the velocity potential is solved, the transient wave pressure over the wetted surface of the vertical
148 wall can be calculated from the following Bernoulli's equation,
149

$$P = -\rho \frac{\partial \phi}{\partial t} - \frac{1}{2}\rho |\nabla \phi|^2 - \rho g z \tag{6}$$

150 where ρ is the density of water. One of challenges in fully nonlinear numerical simulations is the
151 calculation for the time derivative of the velocity potential ϕ_t in Eq. (6). There are several methods for
152 calculating ϕ_t among which the backward finite difference technique is the simplest and is widely applied.
153 However, it is unstable in most cases, especially for the cases with objects moving or piercing through
154 the free surface [34]. In the present study, the so-called acceleration potential method is applied.

155 In the acceleration potential method, as the velocity potential ϕ the temporal derivative of the velocity
156 potential ϕ_t satisfies the Laplace equation in the fluid domain Ω and the impermeable boundary condition
157 on the flume bottom Γ_d as well as the vertical end-wall Γ_r. On the free surface Γ_f, ϕ_t satisfies the Bernoulli
158 equation,

159 $$\frac{d\phi}{dt} = -g\eta + \frac{1}{2}|\nabla \phi|^2 \ . \tag{7}$$

160 The boundary integral equation to be solved for ϕ_t is,

161 $$C(p)\phi_t(p) = \int_\Gamma (\phi_t(p)\frac{\partial G(p,q)}{\partial n} - G(p,q)\frac{\partial \phi_t(p)}{\partial n})\mathrm{d}\Gamma \ . \tag{8}$$

162 Once ϕ_t is obtained, the wave pressure can be calculated from Eq. (6). Then the wave loads can be
163 obtained from the integration of wave pressure along the wetted surface. More details in the numerical
164 schemes and formulations can be found in the references [35].

165

166 3 Validation and Discussions

167 3.1. Comparisons with experimental data

168 In this section, the extended numerical model described above is used to reproduce the published
169 benchmark experiments in [13, 40] on regular waves and focused wave groups impacting on a vertical
170 wall, respectively. Comparisons with the experimental data and the analytical solutions are carried out
171 to assess the performance of the present numerical model when applied to non-linear wave interactions
172 with a vertical seawall for ranges of wave conditions.

173 In [13], a range of regular waves with varying wave steepness and wave frequencies were generated to

impact a model vertical seawall installed at the downstream end of the flume in laboratory. The water depth d was 0.315 m in all tests and four pressure transducers were installed at 0, 6.3, 12.6 and 18.9 cm below the still water level (SWL) to record the pressure distribution along the vertical seawall, *i.e.* z/d = 0.0, -0.2, -0.4, and -0.6. Numerical results for two regular waves with wave period T = 0.55 s and 0.87 s are discussed in this paper. The wave amplitudes are 0.0064 m and 0.0241 m, respectively.

In order to reproduce the experiments, a 2-D numerical wave tank is setup. The length of the numerical wave tank is set as 10λ in which λ is the wavelength. Convergence tests are carried out to determine the optimal time steps and the spatial steps, which are $\Delta t = T/50$ and $\Delta x = \lambda/15$ in this study, respectively. The distribution of dynamic pressures P along the height of the vertical seawall due to regular waves is shown in Fig. 2 for two selected wave conditions. The pressure is normalized by γH in which $\gamma = \rho g$, ρ is the water density, g the acceleration due to gravity and H the wave height. Both numerical results and experimental data are included as well as the solutions of linear theory. For cases with small incoming wave amplitude as shown in Fig. 2(a) (*i.e.*, kA = 0.084, kd = 4.33), noises might be picked up in the experimental measurements. The small deviations of both linear and nonlinear solutions from the measurements are expected. The agreements with the experimental data are satisfactory for both the fully nonlinear potential flow theory and linear theory. While for a relative large wave (*i.e.*, kA = 0.135, kd = 1.77) shown in Fig.2 (b), the linear theory over-predicts the pressure due to strong wave nonlinearity and full reflection from the rigid wall. From Bernoulli equation (Eq. (6)), the wave dynamic pressure on the vertical wall is the function of the wave height. Full reflection assumption in the linear theory results in larger wave crest of reflected waves, thus, larger dynamic wave pressure. Additionally, the total wave dynamic pressure consists of nonlinear wave pressure components at frequencies both lower and higher than the incoming waves in the framework of non-linear wave theory. There is phase difference among wave pressure components which could lead to reductions in dynamic wave pressure on the vertical wall. As seen in Fig. 10, the 2nd order difference term can be 180° out of phase with the linear component. As anticipated, favorable agreement between the fully non-linear numerical results and the experimental data is achieved even for the case where nonlinearity dominates. This confirms the capability of the present numerical model in predicting non-linear regular wave interactions with a vertical seawall in coastal areas.

To further validate the present numerical model, a series of experiment on focused wave groups acting on a vertical wall was performed in a flume (50 m × 3 m × 1m) at Dalian University of Technology. The static water depth for the tests was 0.5 m. The incident focused waves were generated by a hydraulically driven piston-type wave-maker at upstream end of the flume, and were supposed to be focused at x =

14.16 m, which is the stagnation point of the model vertical wall. The dimensions of the model vertical wall were 0.5 m × 3 m × 0.85 m (length in longitudinal direction × width × height in vertical direction). 15 pressure sensors were used to measure the pressure distribution along the surface of the model vertical wall as well as the time histories at certain points. In the experiments, a constant-steepness wave spectrum was applied, so the amplitude of *i*th wave component a_i can be calculated as follows,

$$a_i = \frac{A}{k_i \sum_{i=1}^{N} 1/k_i} \tag{7}$$

where A is the linear crest value of incident focused wave groups, k_i the wave number of *i*th wave component, and the total number of wave components N was selected as 29 in the experiment. In the numerical simulations, the target focal position was x_p =15 m and the target focal time was defined as $x_p/t_p = \lambda_{min}/2T_{min}$ in which λ_{min} and T_{min} are the shortest wavelength and the smallest wave period of wave components, respectively. But there was some shift in this focusing because of the nonlinear dispersion of the focused wave groups. The present numerical model is carefully calibrated to ensure all focused wave groups are approximately focused at the upstream stagnation point of the vertical wall. In the numerical simulations, the spatial and the time steps are selected as $\Delta x=\lambda_{min}/15$ and $\Delta t=T_{min}/50$, respectively according to the convergence tests.

Fig.3 shows both the numerical and measured time histories of the free surface elevation at focused point without the presence of the vertical seawall. Here, the linear crest value of the focused wave group A = 0.076 m, and the wave frequency f = (0.65 Hz, 1.35 Hz) and (0.6 Hz, 1.5 Hz), respectively. In this study, uniform increment in frequency between adjacent wave components is applied, *i.e.* $f_{step} = f_{i+1} - f_i$ is the same for all wave components. That is, take f = (0.65 Hz, 1.35 Hz) as example, the upper and lower frequencies are 0.65 and 1.35 Hz, respectively, and f_{step} = (1.35-0.65)/29 = 0.024 Hz. The difference between the upper and lower frequencies is defined as the wave spectrum bandwidth, *i.e.* the wave spectrum bandwidths in Fig. 3 (a) and (b) are 0.7 and 0.9 Hz, respectively. From the figures, it can be seen that there is good agreement between the experimental data and numerical results, with similar values and phases. The peak wave crests increase to 0.089 m and 0.11 m for broad-banded and narrow-banded cases, respectively, due to nonlinear evolution in waves.

The time series of the wave pressure on the vertical wall at z = 0.05 m above the mean water level are shown in Fig.4 for both narrow- and broad- banded cases. Characteristic ‘one-peak’ profiles are observed in both numerical and experimental results for both cases, with short duration time. There is a favorable agreement for pressure maxima and it is noted that the rise time, which is defined as the time needed to

rise the pressure from zero to its maximum value, is larger in numerical results. The rise time predicted by the present numerical model is approximately 0.3 ~ 0.4 s, while is almost zero in model tests resulting in very sharp impacts. This difference could be due to several reasons, including the accuracy of the pressure sensor in measuring such short duration loads and the possible trapped air pocket. An empirical formula $P_{max} = at^b$ was proposed by Weggel and Maxwell [38] to determine the relationship between maximum impact pressure and the rise time. a and b are non-dimensional empirical coefficients which are advised to be 232 and -1 in [38], respectively. It is found that the numerical results follow the empirical formula with $P_{max} \sim 0.53$ kPa. The total impact duration is about 0.27 s for both cases which is shorter than the forming time of the focused wave crest (i.e., the temporal interval between two neighboring equilibrium positions of the focused wave crest, about 0.40 s), as shown in Fig.3. Additionally, the total impact duration and the rise time for both cases with different bandwidth are almost the same, indicating that the effect of bandwidth on the total impact duration and the rise time is small at least for the studied wave conditions.

Fig. 5 shows distributions of the normalized wave pressure along the vertical seawall. A^* is the actual crest value of the focused wave group, *i.e.* the undisturbed nonlinear crest of the focused wave group at actual focal point without the presence of the vertical seawall. As with the regular wave conditions, the agreements between the predicted and measured dynamic pressure on the vertical seawall due to focused wave groups are generally good, with similar values and profiles. This indicates that the present numerical model is able to capture main physics that involved in the process of focused wave groups interaction with a vertical seawall in shallow water regions. For the wave and geometry conditions investigated in this study, the maximum pressure is observed to occur at the mean water level in both numerical simulations and the experiments. This is consistent with what has been observed in [39] in which the locations of both the maximum quasi-static loads and impact loads are in the vicinity of the mean water level.

In the sections to follow, the validated numerical model is used to investigate the effects of the wave spectrum bandwidths, the wall positions and the wave nonlinearity on the wave run-up and the maximum wave pressure on the vertical seawall.

3.2. The effect of the vertical seawall on the wave run-up and the pressure

Fig. 6 shows time series of the free surface elevation at focal point for cases with and without the vertical seawall in place. The linear crest value of the focused wave group is $A = 0.06$ m with f = (0.65 Hz, 1.35 Hz). The results for the case with the vertical wall in place are shown in the left column and the results

for the case without the vertical wall are shown in the right column. It can be seen that the peak free surface elevation in the case with the vertical wall in place is approximately 2.6 times of that without the seawall. This increase in the free surface elevation is even larger than that resulting from a perfect reflective vertical wall (which is approximately twice the height of the incident wave group). The possible reason for the enhanced response is the nonlinear interaction of the incoming wave groups with the vertical wall.

Time series of the free surface elevations at the focal point for the incident wave groups with the linear crest value A = 0.01 m and 0.06 m are shown in Fig. 7 (a) and Fig. 7 (b), respectively. The results for the cases with and without the vertical wall are included. The free surface elevations for the cases in absence and presence of the vertical wall are normalized by A and 2A, respectively. It can be seen that for the small wave amplitude, the full reflection due to the vertical wall gives a combined wave with wave height of approximately twice the wave height of the incident wave group. And for the large wave amplitude with the vertical wall, the reflected wave amplitude is about 1.3×2A as shown in Fig. 7 (b). The corresponding semi-log plots of the power spectra for the free surface elevation (shown in Fig. 7) are shown in Fig. 8. The frequency in horizontal axes is normalized by the central frequency f_c. It is clearly seen from the power spectra that sub- and high- harmonics components exist for the case with large wave amplitude. This is attributed to the nonlinearity in waves and interactions between waves and structures. .

The harmonic structure of the free surface run-up on the vertical seawall can be extracted by a phase-based harmonic separation method presented in [23, 24, 28]. In the phase-based separation method (*i.e.* the 'phase-inversion' method), the Stokes wave expansion in regular waves is extended to focused wave groups by assuming the existence of a Stokes-like harmonic series in both wave steepness and frequency for the free surface elevation of focused wave groups. The application of the 'phase-inversion' method requires free surface elevation time series for a focused wave group and the same wave group inverted, which are out of phase with each other. The total free surface elevation is then separated into odd and even harmonics by doing subtraction and addition to the free surface elevation time series. This makes the adjacent harmonics within both spectra for odd and even terms much further apart in frequency so as to allow a clean separation of the focused wave groups into its fundamental components by digital filtering.

Fig. 9 shows the extracted harmonic structures of the free surface elevation at the focal point for cases with and without the vertical seawall in place. The linear crest value of the focused wave group is A = 0.06 m with f = (0.75 Hz, 1.25 Hz). From the top to bottom are the long wave, linear and 2nd harmonics, and the left and right column show the results for the cases with and without the vertical wall in place,

respectively. The harmonics of the free surface elevation are enveloped to display the energy distribution in time. The envelope of the fundamental component is obtained by applying the Hilbert transform and the envelope of each harmonic above 2nd order is derived from the envelope of the linear component, as described in [23] among others.

It can be seen from Fig. 9 that the applied phase-inversion separation method works well, and the extracted harmonics and the estimated envelopes agree well with each other. The focusing time of the incoming wave groups is about ~17s for both cases with and without the vertical seawall in place. It is also found that the existence of the vertical seawall leads to an increase in the free surface elevation for all harmonics, but the amount of the increase decreases from long wave to the second-order harmonics. The peak values in the free surface elevation from long wave to the second-order harmonics for the cases with the vertical seawall in place are about 2, 1.33 and 0.33 times larger than their counterparts for the cases without the vertical wall in place. In addition, there is a phase difference of π in long waves from set-down to set-up, which indicates that the wave-induced perturbation of the mean water level is different because of the existence of the vertical seawall.

Additionally, it can be seen that contributions of higher order free surface elevation above the first-order are about 14% and 20% of the total free surface elevation for the cases without and with the vertical wall in place, respectively. This indicates that the linear potential flow theory is applicable for small waves. However, for large waves, where wave nonlinearity dominates, the use of the linear potential flow theory is inadequate and would lead to a loss of a considerable percentage of energy.

The same analysis is performed for the wave loading on the vertical seawall and the results are shown in Fig. 10. The wave conditions are the same as those in Fig. 9. For the cases without the vertical seawall in place, the undisturbed pressures at location of the vertical seawall in the absence of the vertical seawall are recorded and integrated, *i.e.* an artificial vertical seawall is placed. Similar phenomena in Fig. 9 have been observed, and compared with the free surface run-up, the non-linear effect on the wave loading is less significant, with only 77% increase in the linear wave loading. Similar conclusion has been presented in [28] in which focused wave group interactions with a vertical cylinder was investigated using viscous flow theory. Additionally, a phase difference of 180 degrees was observed between the second-order difference terms of the free surface elevation and wave loading.

The effect of the vertical seawall is further studied by varying the wall position. Fig.11 shows time series of the wave run-ups on a vertical seawall that is located at three different positions, $L_1=x_f-2\lambda_{min}$, $L_2=x_f$ and $L_3=x_f+2\lambda_{min}$. It means that the vertical seawall is placed right at the focal position for L_2, and is

moved $2\lambda_{min}$ forward and backward for L_1 and L_3, respectively. The wave conditions are the same as those in Figs. 7 and 8. It can be seen that the most violent wave-structure interaction occurs when the focal position of the focused wave group is at the stagnation point of the vertical seawall, *i.e.* the vertical seawall is placed right at the focal position L_2. For small waves that can be treated as linear waves, as shown in Fig. 11 (a), the wave shape for wave run-up on the vertical seawall at location of L_2 is symmetrical about the focusing event, while asymmetric shapes are observed in the wave run-up when the vertical seawall is placed at L_1 or L_3. This process is close to the evolution of a focused wave group in a pure wave tank without structures in place, as presented in [36]. With the increase of wave nonlinearity, the asymmetry in the surface profile becomes increasingly significant as shown in Fig. 11 (b). The asymmetry occurs even for the wave run-up on the vertical seawall at location of L_2 as wave nonlinearity increases.

Fig.12 shows the distribution of normalized peak pressures along the height of the vertical seawall at three different locations. The wave conditions and the wall positions are the same as those shown in Fig. 11. It can be seen from the figures that the maximum peak pressure occurs when the vertical seawall is placed at the focal point L_2. At the adjacent locations (L_1 and L_3), the peak pressures are reduced, but they close to each other up to the area near the mean water level.

The effect of the location of vertical seawall is considered in details in Fig. 13 in which variations of the crest wave run-up and the maximum wave loading on the vertical seawall with the locations of the vertical seawall are shown. The actual focal point is x_f and the vertical seawall is moved from $-4\lambda_{min}$ to $+4\lambda_{min}$ away from the focal point. The sign negative and positive mean that the vertical seawall is moved backwards and forwards, respectively. It can be seen that the wave run-up and the wave loading on the vertical seawall at the focal point are the largest compared with the results for the cases that the vertical seawall is located away from the focal point, consistent with what is observed from Figs. 11-12. It is clear that the direction of the wall movement has relatively weak effects on the run-up and the wave loading as the variations of the run-up and the wave loading are approximately symmetrical about the focal point. Additionally, differences in the wave run-up and the wave loading on the vertical seawall because of the movement of the vertical seawall is larger for incoming focused wave groups with larger linear crest amplitude due to stronger wave nonlinearity. As anticipated, differences in the wave run-up is more obvious than that in wave loading, which indicates that the wave nonlinearity in wave loading is less significant as observed in Figs. 9-10.

The evolution of the focused wave group in the presence of vertical seawall is considered in Fig. 14. Two linear incoming wave amplitudes are considered (A = 0.01 m and 0.06 m) for the spectrum f = (0.65Hz,

1.35Hz). t_f is the actual focal time and the time increment dt = 0.0148 s. Fig. 14 shows the convergence of wave energy at the focal time and the rapid development of the maximum crest run-up on the vertical seawall.

3.2. The effect of wave parameters on the wave run-up and the pressure

In this section, the validated numerical model is used to study the dependence of the maximum wave run-up and the pressures on surrounding sea states. Spectrum bandwidth is one of the most important parameters that affect the characteristics of the incoming focused wave groups. Fig. 15 considers the surface elevations resulting from wave groups with three different spectrum bandwidths. (*i.e.*,0.75 Hz $\leq f \leq$ 1.25 Hz, 0.65 Hz $\leq f \leq$ 1.35 Hz, 0.55 Hz $\leq f \leq$ 1.45 Hz). Two incident linear wave amplitudes are considered (A = 0.01 m and 0.06 m). The linear focal positions x_p are selected as 12 m, 15 m and 18 m for spectrum bandwidth BW = (f_{max} - f_{min}) of 0.5 Hz, 0.7 Hz and 0.9 Hz, respectively. The corresponding focal times are defined according to the formula $x_p/t_p=\lambda_{min}/2T_{min}$. With a small input amplitude (Fig. 15 (a)), there is a good agreement between the numerical results for the extreme crest, all equal to twice incident amplitude A and the envelopes are symmetric about the focal time. In this case, the amplitude of the individual wave components is less than 1 mm (calculated by Eqn. (13)), and, consequently, the non-linear wave-wave interactions are negligible. However, for a larger incident wave A = 0.06 m in Fig.15 (b), the increase in wave amplitude leads to a divergence from the linear solution. The maximum crest run-up on the vertical seawall reaches 0.185 m for BW = 0.5 Hz, about 1.5 times the linear solution due to strong wave nonlinearity. The wave crest at the focal position becomes large, and the adjacent wave troughs become deeper for narrow-banded spectrum. In addition, it can be seen that the wave crest decreases with increasing spectrum bandwidth for both considered input wave amplitude, though, it is more obvious for larger input wave amplitude due to stronger non-linearity. Larger spectrum bandwidth leads to larger incident wave energy and more violent energy transfer between adjacent harmonics [40]. The phase difference between harmonics could lead to the reduction in the total surface elevation, as shown in Fig. 2 and Fig. 9. The mutual effect of the increasing incident wave energy and larger harmonics at frequencies lower and higher than the linear component results in smaller wave crest for cases with a broader bandwidth.

Fig.16 shows the distribution of the peak wave pressure along the height of the vertical seawall at focal time for wave groups with three different spectrum bandwidths. The wave conditions are the same as those in Fig. 15. It can be seen from Fig.16 that the peak pressure on and below the still water level

increases with the spectrum bandwidth, which is opposite to what has been observed in Fig. 15. This may due to the fact that there are phase differences between the linear surface elevation and the linear wave pressure as well as the corresponding sub- and higher-harmonics. Similar to the wave run-up, the differences in peak pressure resulting from the differences in spectrum bandwidth are more obvious in the cases with larger input wave amplitude.

The effect of input linear wave amplitude A on the maximum crest elevation and the maximum wave loading is investigated in Fig. 17. Three spectrum bandwidths are considered (BW = 0.5 Hz, 0.7 Hz and 0.9 Hz). From the figure, it is found that the increased wave amplitude produces a rapid divergence from the linear solution especially when A > 0.03 m. And the maximum wave run-up in the narrow-banded case is larger than that in the broad-banded case with the same input linear wave amplitude. Opposite trend is observed in the maximum wave loading. This trend is more obvious for the cases with larger input amplitude A, as observed in Figs. 15-16.

4. Conclusions

A time-domain numerical model based fully nonlinear potential flow theory is extended and applied in this study to investigate the performance of coastal structures with vertical wall in extreme events. The fully nonlinear wave motion is captured using a mixed Eularian-Lagrangian higher-order boundary element method, and it is advanced in time by applying 4th-order Runge-Kutta technique to the fully nonlinear kinematic and dynamic free surface boundary conditions. New boundary conditions are added to extend capabilities of the numerical model in generating focused wave groups so as to allow an investigation of focused wave group interactions with a vertical seawall. The numerical model has been validated by comparing with the published benchmark experiments on both non-linear regular waves and focused wave groups impacting on a vertical seawall.

The characteristics of maximum wave run-up and consequent maximum wave pressure on the vertical seawall are investigated in depth using the validated numerical model. It is found that not only the reflection from the vertical seawall but also the wave nonlinearity contributes to the increase of the maximum crest wave elevation and wave pressure. The maximum wave run-up on the vertical seawall can be 2.6 times the height of the incident wave group with larger incident wave amplitude. Also, the wave nonlinearity is found to increase with deceasing bandwidth. This indicates that the increased wave amplitude and the decreased bandwidth would produce a rapid divergence from the linear solution. In the cases where wave nonlinearity dominates, the use of linear theory is not adequate and leads to an underestimation in the maximum wave run-up and overestimation in the maximum pressure on the

vertical seawall, respectively. That is, the application of the fully nonlinear potential flow theory is necessary and important for practical applications where wave nonlinearity is significant. The proposed numerical model is also appropriate for other applications such as green waters and dynamic responses of floating structures.

Further investigation by extracting the harmonic structures of the maximum wave elevation and wave loading on the vertical seawall found that the existence of the vertical seawall relates to the generation of both sub- and higher harmonics, and their contributions can be large, up to 20%. Additionally, compared with the free surface elevation, the nonlinear effect on wave pressure and wave loading on the vertical seawall is less significant, with a smaller increase for the same wave condition.

Furthermore, most violent wave-structure interactions are observed when the focal point is at the vertical seawall, *i.e.* the vertical seawall is placed right at the focal point. Moving the structure either forwards or backwards reduces both the maximum crest elevation and pressure on the vertical seawall. The effect of the direction of movement is negligible in the present study.

Acknowledgements This work was supported by the National Natural Science Foundation of China (Grant Nos. 51679036 and 51490672) and Royal Academy of Engineering under the UK-China Industry Academia Partnership Programme (Grant No.UK-CIAPP \ 73).

REFERENCES

[1] J.K. Mallory, Abnormal waves on the south east coast of South Africa. Int. Hydrog. Rev. 51 (1974) 99–129.

[2] I.V. Lavrenov, The wave energy concentration at the Agulhas current of South Africa. Natural Hazards, 17 (1998) 117-127.

[3] S.E. Sand, N.E.O. Hansen, P. Klinting, O.T. Gudmestad, M.J. Stemdorff, Freak wave kinematics. In: Torum, A., Gudmestad OT (Eds.), Water wave kinematics, Kluwer Academic Publishers, Dordrecht, The Netherlands, 1990, PP. 535-549.

[4] A.B. Rabinovich, S. Monserrat, Generation of meteorological tsunamis (large amplitude seiches) near the Balcaric and Kuril Islands, Natural Hazards, 18 (1998) 27-55.

[5] R.G. Dean, R.A. Dalrymple, Coastal Processes with Engineering Applications, Cambridge University Press, 2002.

[6] H. Chien, C.C. Kao, L.Z. Chuang, On the characteristics of observed coastal freak waves, Coast. Eng. J. 44 (2002) 301–319.

[7] I. Didenkulova, A.V. Slunyaev, E.N. Pelinovsky, C. Kharif, Freak waves in 2005, Natural Hazards and Earth System Sciences, 6 (2006) 1007-1015.

[8] I. Nikolkina, I. Didenkulova, Rogue waves in 2006-2009, Natural Hazards Earth System Sciences, 11 (2011) 2913-2924.

[9] L. O'Brien, J.M. Dudley, F. Dias, Extreme wave events in Ireland: 14 680 BP–2012, Natural Hazards Earth System Sciences, 13 (2013) 625–648.

[10] V. Sundar, K.V. Anand, Dynamic pressure and run-up on curved seawalls compared with vertical wall under cnoidal waves, Indian Journal of Marine Sciences, 39 (2010) 579.

[11] M.S. Kirkgoz, Impact of breaking waves on vertical and sloping walls, Ocean Engineering, 18 (1991) 45-59.

[12] Y. Goda, The fourth order approximation to the pressure of standing waves, Coastal Engineering in Japan, 10 (1967) 1-11.

[13] V. Mallayachari, V. Sundar, Standing wave pressures due to regular and random waves on a vertical wall, Ocean Engineering, 22 (1995) 859-879.

[14] D. Kisacik, P. Troch, P. Van Bogaert, Experimental results of breaking wave impact on a vertical wall with an overhanging horizontal cantilever slab, in: 32nd International Conference on Coastal Engineering (ICCE), 30 June - 5 July 2010, Shanghai, China.

[15] Y.J. Lin, Dynamic Behavior of Vertical Breakwater Induced by Regular Waves, Master Theses, Department of Harbor and River Engineering, National Taiwan Ocean University, 2004.

[16] S. Komori, H. Tanaka, A. Wada, Simulation method of ocean wave spectra in an experimental basin and its application to the study on wave pressures, Coastal Engineering Japan, 21 (1978), 51-61.

[17] Y.F. Chiu, J.G. Lin, S.C. Chang, Y.J. Lin, C.H. Chen, C.H., An experimental study of wave forces on vertical breakwater, Journal of Marine Science and Technology, 15 (2007) 158-170.

[18] G. Cuomo, W. Allsop, T. Bruce, J. Pearson, Breaking wave loads at vertical seawalls and breakwaters, Coastal Engineering, 57 (2010) 424-439.

[19] Y. Goda, Random seas and design of maritime structures, 2nd Edition, Advanced Series on Ocean Engineering, World Scientific, 15 (2000) 443.

[20] N.W.H. Allsop, D. Vicinanza, J.E. McKenna, Wave forces on vertical and composite breakwaters, Strategic Research Report SR 443, HR Wallingford, 1996, pp. 1–94.

[21] P.S. Tromans, A. Anaturk, P. Hagemeijer, A new model for the kinematics of large ocean waves – application as a design wave, Proceedings of the 1st International Offshore and Polar Engineering, 3 (1991) 64-71.

[22] P. Jonathan, P.H. Taylor, P.S. Tromans, Storm waves in the northern North Sea, Proc. Conf. on the Behaviour of Offshore Structures, BOSS'94, Boston, USA, 2 (1994) 481–494.

[23] T.E. Baldock, C. Swan, P.H. Taylor, A laboratory study of nonlinear surface waves on water, Phil Trans R Soc Lond A, 354 (1996) 649-676.

[24] A.G.L. Borthwick, A.C. Hunt, T. Feng, P.H. Taylor, P.K. Stansby, Flow kinematics of focused wave groups on a plane beach in the U.K, Coastal Research Facility, Coastal Engineering, 53 (2006) 1033-1044.

[25] H. Bredmose, N.G. Jacobsen, Vertical wave impacts on offshore wind turbine inspection platforms, Proc Int Conf on Ocean, Offshore and Arctic Engineering, Rotteram, OMAE2011, 5 (2011) 645-654.

[26] X.Z. Zhao, C.H. Hu, Numerical and experimental study on a 2-D floating body under extreme wave conditions, Applied Ocean Research, 35 (2012) 1-13.

[27] T. Vyzikas, E. Ransley, M. Hann, D. Magagna, D. Greaves, D. Simmonds, V. Magar, D. Conley, Integrated numerical modeling system for extreme wave events at the wave hub site, Proc of the ICE Conf: Coasts, Marine Structures and Breakwaters, Edinburgh, 2013.

[28] L.F. Chen, J. Zang, A.J. Hillis, G.C.J. Morgan, A.R. Plummer, Numerical investigation of wave-structure interaction using OpenFOAM, Ocean Engineering, 88 (2014) 91-109.

[29] D. Stagonas, E. Buldakov, R. Simons, Focusing unidirectional wave groups on finite water depth with and without currents, Proc Int Conf on Ocean, Offshore and Arctic Engineering, Honolulu, OMAE 2009, 2009, pp. 653-660.

[30] T.A.A. Adcock, P.H. Taylor, Non-linear evolution of uni-directional focused wave-groups on a deep water: A comparison of models, Applied Ocean Research, 59 (2016) 147-152.

[31] C.N. Wittaker, C.J. Fitzgerald, A.C. Raby, P.H. Taylor, J. Orszaghova, A.G.L. Borthwick, Optimisation of focused wave group runup on a plane beach, Coastal Engineering, 121 (2017) 44-55.

[32] D.Z. Ning, J. Zang, S.X. Liu, R. Eatock Taylor, B. Teng, P.H. Taylor, Free-surface evolution and wave kinematics for nonlinear uni-directional focused wave groups, Ocean Engineering, 36 (2009) 1226-1243.

[33] R. Dean, R. Dalrymple, Water Wave Mechanics for Engineers and Scientists, Prentice-hall Inc., 1984, pp. 353.

[34] W.C. Koo, M.H. Kim, Freely floating-body simulation by a 2D fully nonlinear numerical wave tank, Ocean Engineering, 31 (2004) 2011-2046.

[35] K. Tanizawa, A nonlinear simulation method of 3D body motions in waves, J Soc Nav Arch Japan, 178 (1995) 179-191.

[36] D.Z. Ning, B. Teng, R. Eatock Taylor, J. Zang, Nonlinear numerical simulation of regular and focused waves in an infinite water depth, Ocean Engineering, 35 (2008) 887-899.

[37] Technical Standards for Port and Harbor Facilities a Japan, Overseas Coastal Area Development Institute of Japan, Tokyo, Japan, 1980.

[38] J.R. Weggel, W.C. Maxwell, Numerical model for wave pressure distributions, Journal of the Waterways, Harbors and Coastal Engineering Division, 96 (1970) 623-624.

[39] G. Cuomo, W. Allsop, T. Bruce, J. Pearson, Breaking wave loads at vertical seawalls and breakwaters, Coastal Engineering, 57 (2010) 1-32.

[40] Y. Wang, The characteristic research and effect on vertical wall of focusing waves, Master thesis, Dalian University of Technology, Dalian, 2007. (in Chinese)

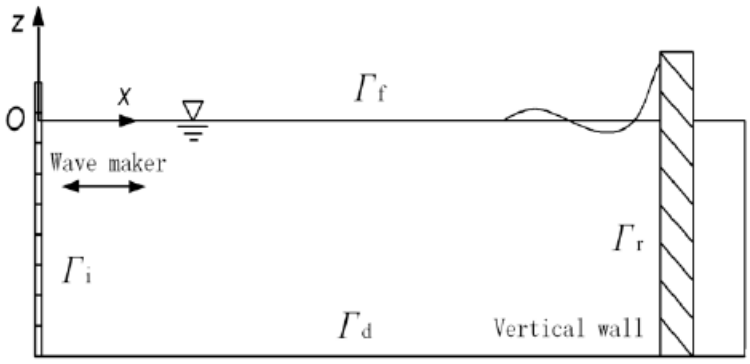

Fig.1 Definition sketch of the wave flume

533
534
535
536
537
538

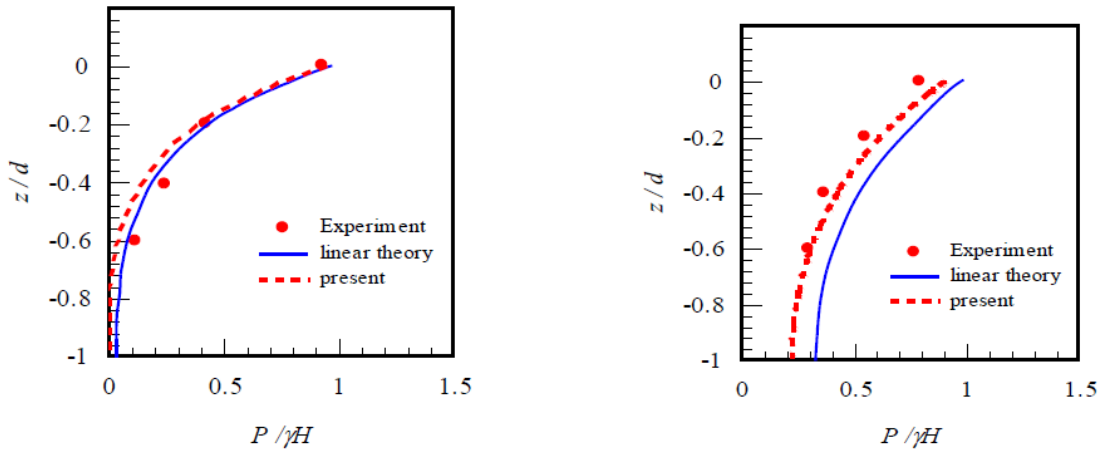

(a) A = 0.0064 m, ω=11.34 *rad/s* (b) A = 0.0241*m*, ω=7.20 *rad/s*

Fig.2 The distribution of normalized pressures along the height of the vertical seawall due to regular waves.

539

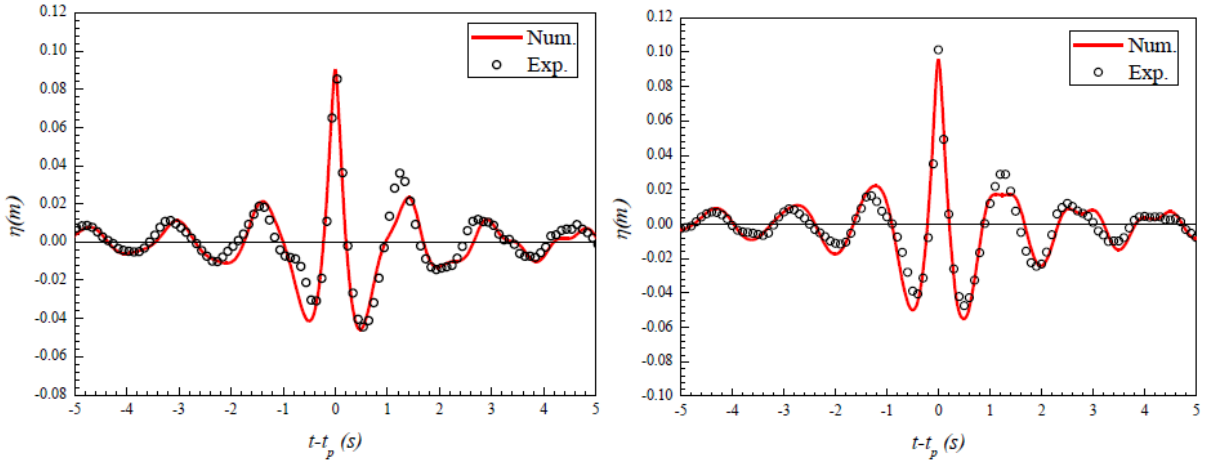

(a) f = (0.6 Hz, 1.5 Hz) (b) f = (0.65 Hz, 1.35 Hz)

Fig.3 Numerical and measured time series of the free surface elevation at the focused point.

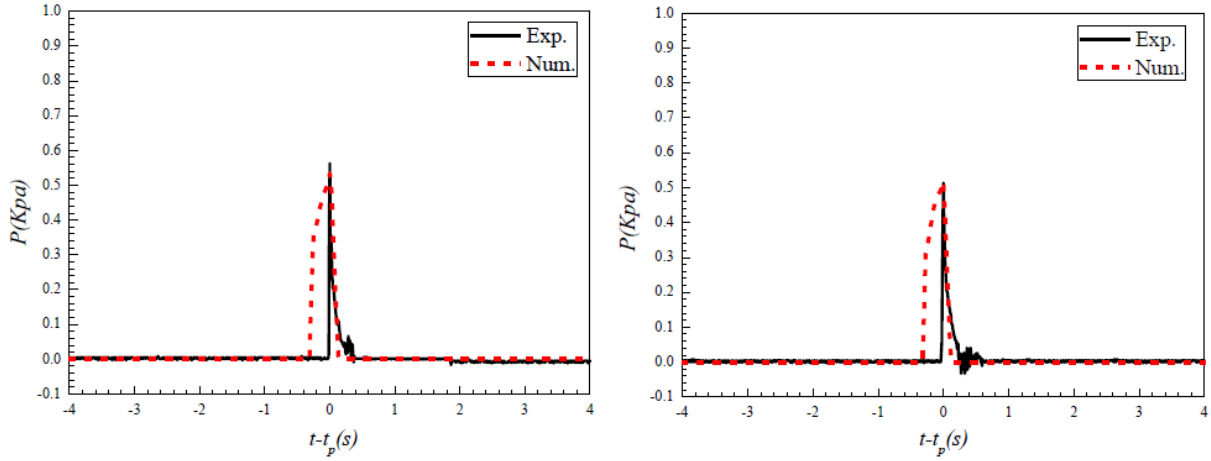

(a) f = (0.6 Hz, 1.5 Hz) (b) f = (0.65 Hz, 1.35 Hz)

Fig.4 Time series of wave pressures on the vertical wall at z = 0.05 m.

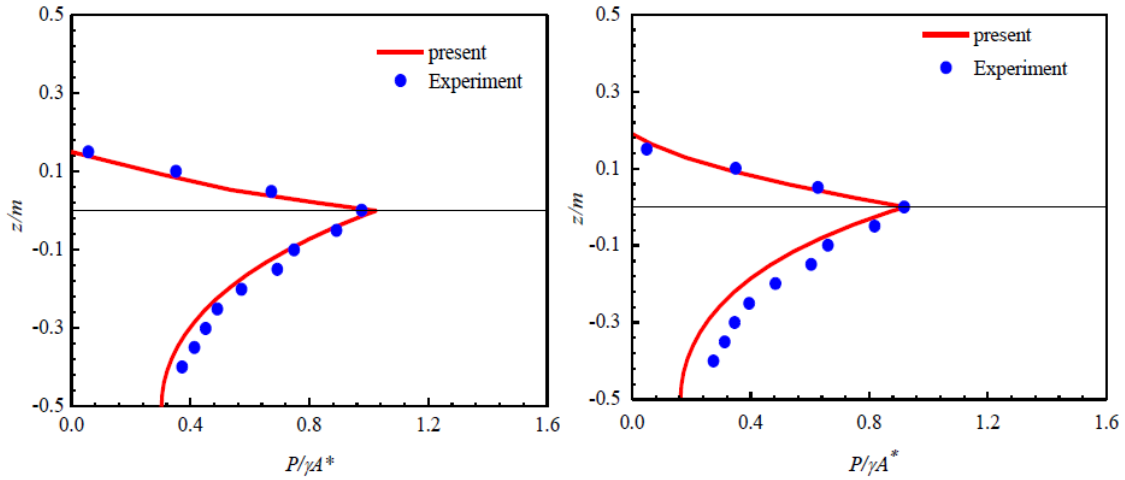

(a) f = (0.6 Hz, 1.5 Hz) (b) f = (0.65 Hz, 1.35 Hz)

Fig. 5 Distribution of wave pressure along the vertical wall

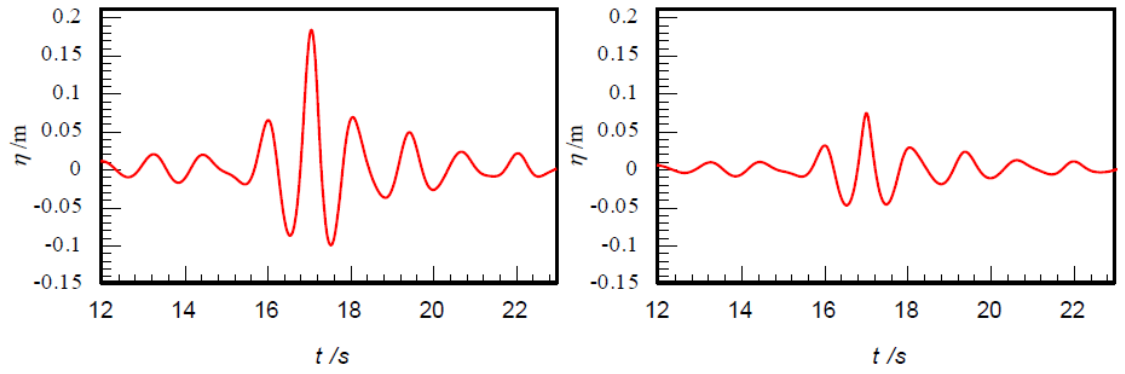

(*a*) with the vertical seawall in place (*b*) without the vertical seawall in place

Fig.6 Time series of the free surface elevation at focal point with and without the vertical seawall in place. The linear crest value of the focused wave group is A = 0.06 m with f = (0.65 Hz, 1.35 Hz). Left: with the vertical seawall in place, Right: without the vertical seawall in place.

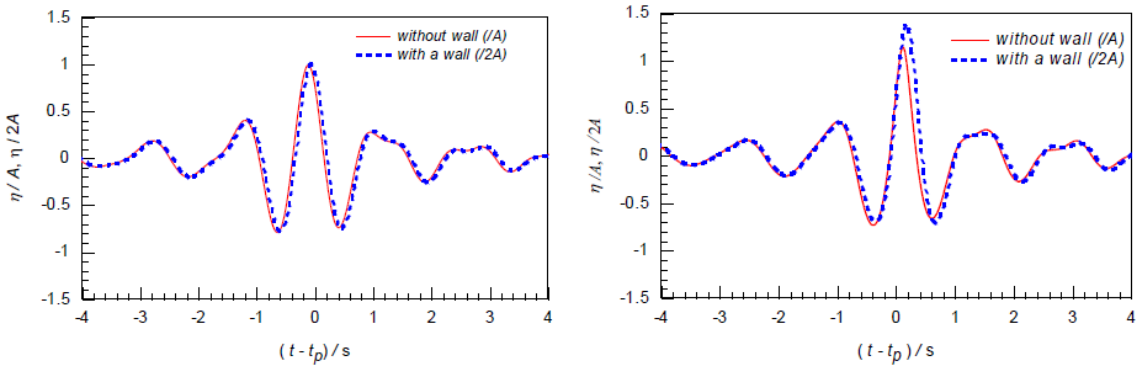

(a) A = 0.01 m (b) A = 0.06 m

Fig.7 Time series of the free surface elevation at focal point with and without the vertical wall in place for the spectrum with f = (0.65 Hz, 1.35 Hz).

555
556
557
558
559
560

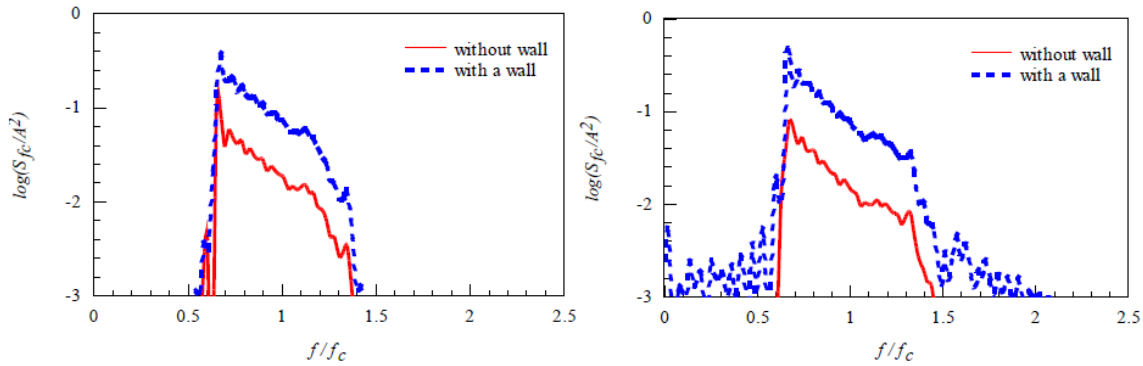

(a) A=0.01 m (b) A = 0.06 m

Fig.8 Power spectra for the free surface elevation time series shown in Fig. 7.

561
562
563

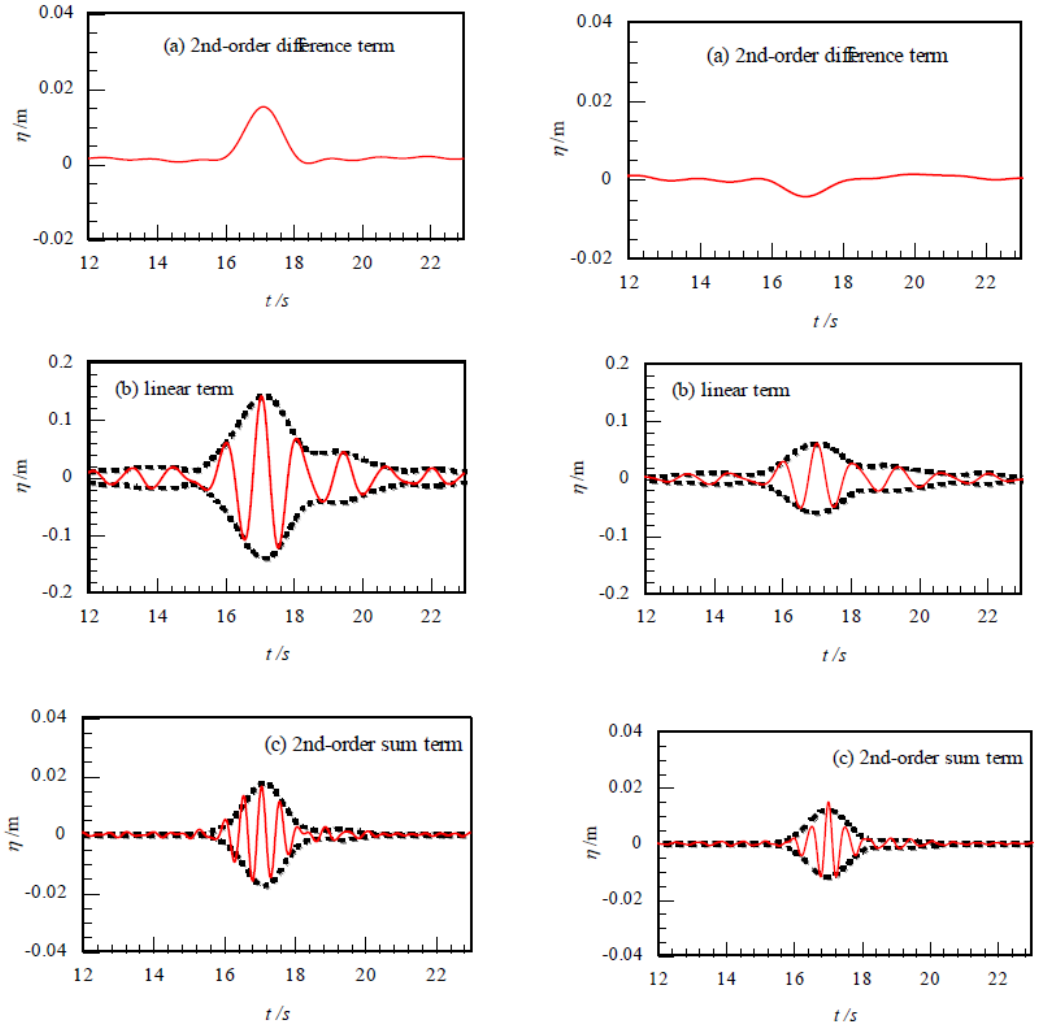

Fig.9 The harmonic structures of the free surface elevation at focal point and envelopes for cases with and without the vertical seawall in place. The linear crest value of the focused wave group is A = 0.06 m with f = (0.75 Hz, 1.25 Hz). Left: with the vertical seawall in place; Right: without the vertical seawall in place.

564
565

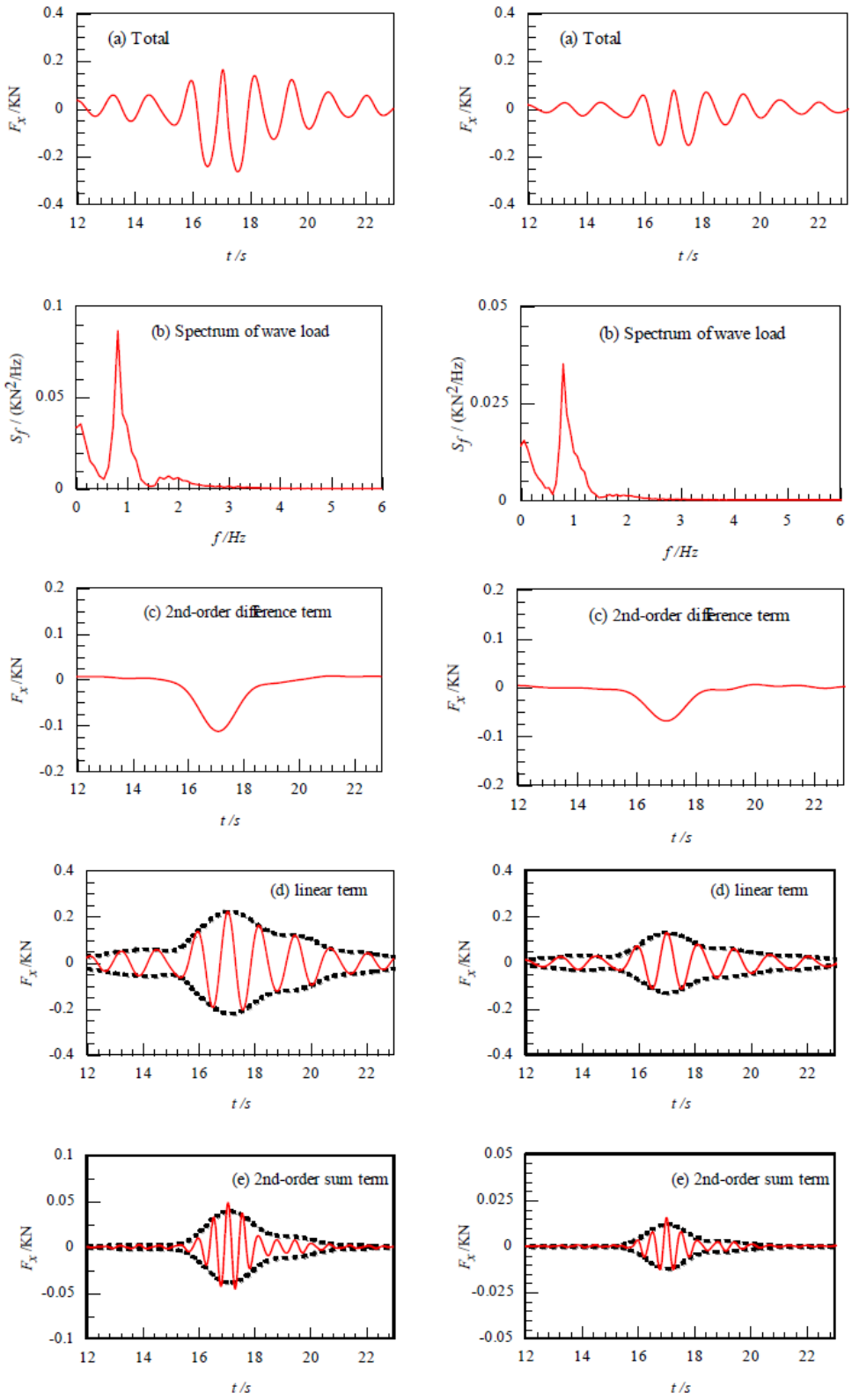

Fig.10 The harmonic structures of the wave loading on the vertical seawall and their envelopes for cases with and without the vertical seawall in place. The linear crest value of the focused wave group is A = 0.06 m with f = (0.75 Hz, 1.25 Hz). Left: with the vertical seawall in place; Right: without the vertical seawall in place.

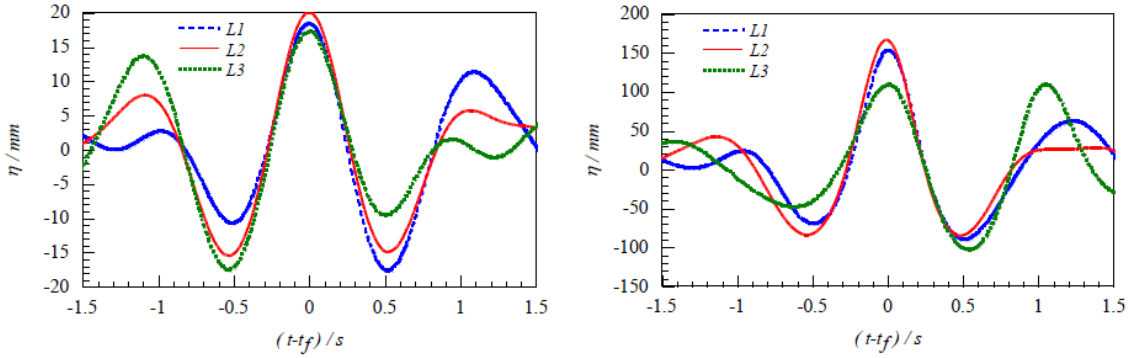

(a) A = 0.01 m (b) A = 0.06 m

Fig.11 Time series of the wave run-up on the vertical seawall at three different wall positions with f = (0.65Hz, 1.35Hz)

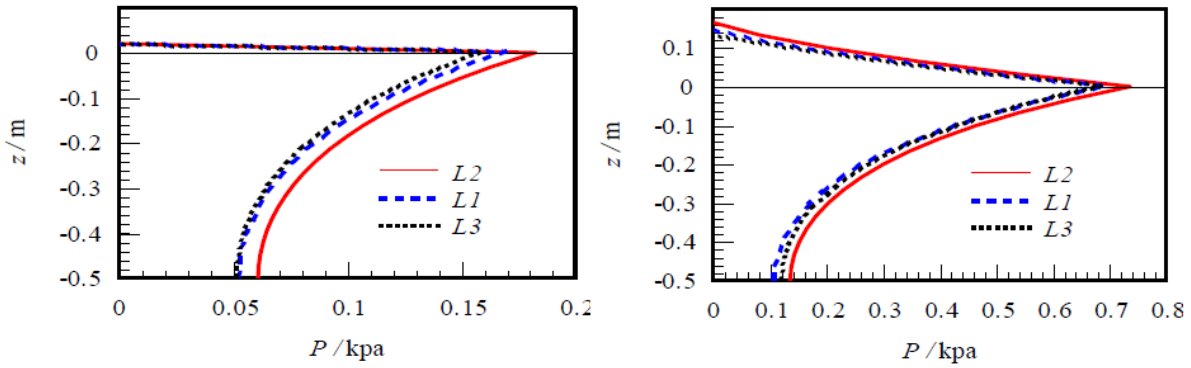

(a) A = 0.01 m (b) A = 0.06 m

Fig.12 The distribution of normalized peak pressures along the height of the vertical seawall at three different wall positions with f = (0.65Hz, 1.35Hz).

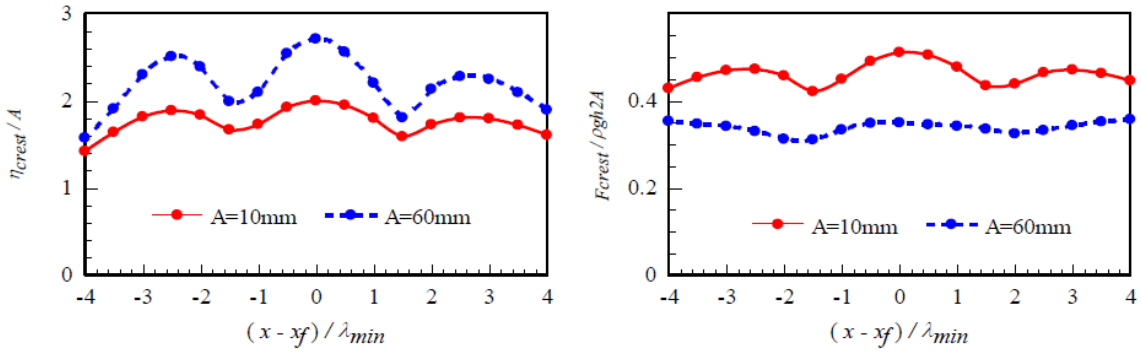

(a) the crest wave elevation (b) the maximum wave load

Fig.13 Variations of the crest wave elevation and the maximum wave loading on the vertical seawall with the locations of the vertical seawall for f = (0.65Hz, 1.35Hz).

575
576
577
578
579
580

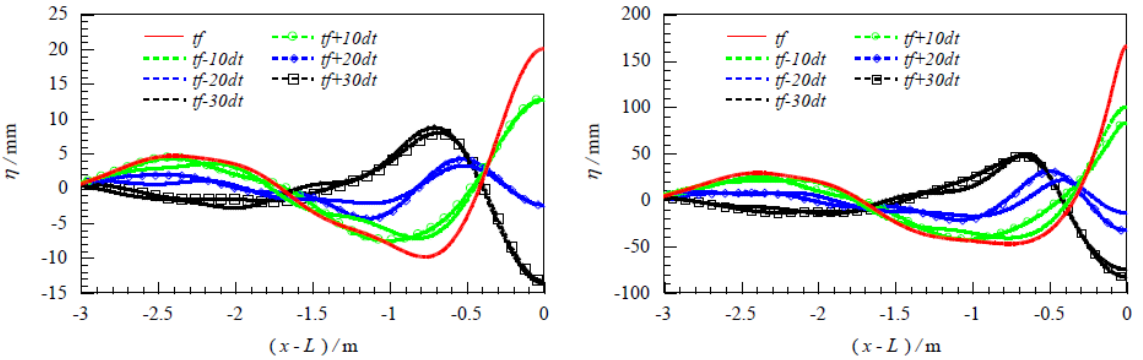

(a) A = 0.01 m, t_f = 26.50 s (b) A = 0. 06 m, t_f = 26.74 s

Fig.14 Evolution of the focused wave groups with the spectrum f = (0.65Hz, 1.35Hz) and the time increment dt = 0.0148 s.

581
582

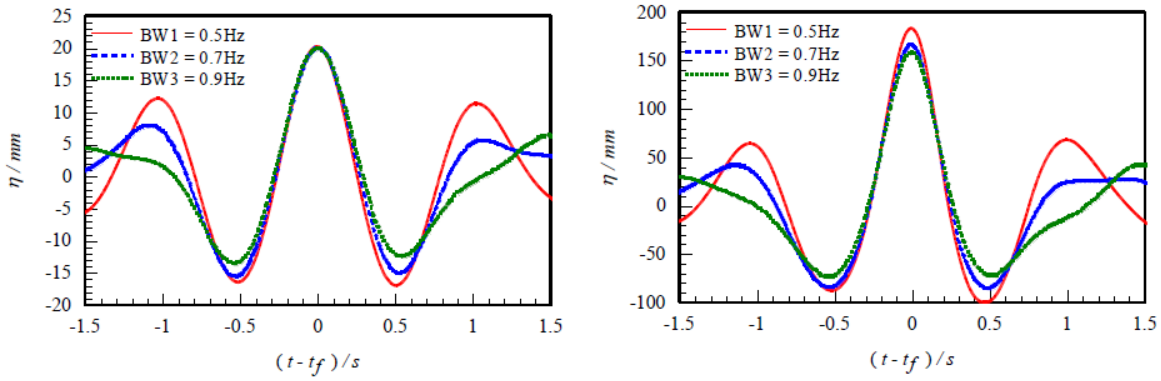

(a) A = 0.01m (b) A= 0.06 m

Fig.15 Time series of the wave run-up on vertical seawall for focused wave groups with various bandwidths.

583
584
585
586
587
588

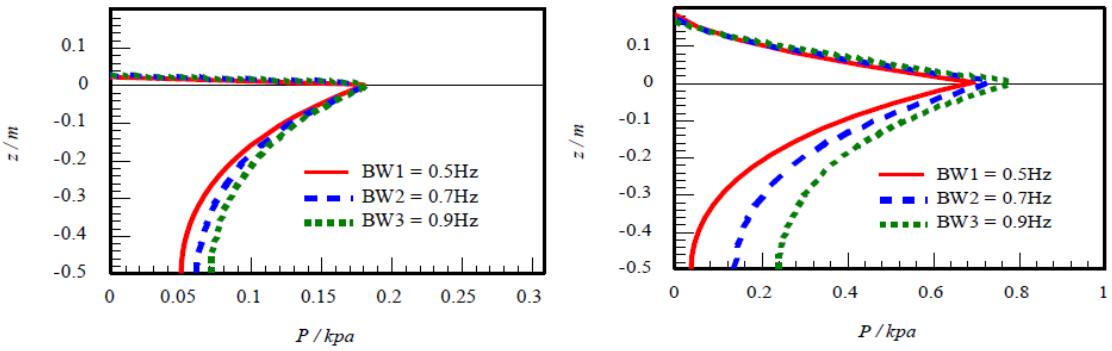

(a) A = 0.01m (b) A = 0.06m

Fig.16 The distribution of the peak wave pressure along the height of the vertical seawall for focused wave groups with various bandwidths.

589

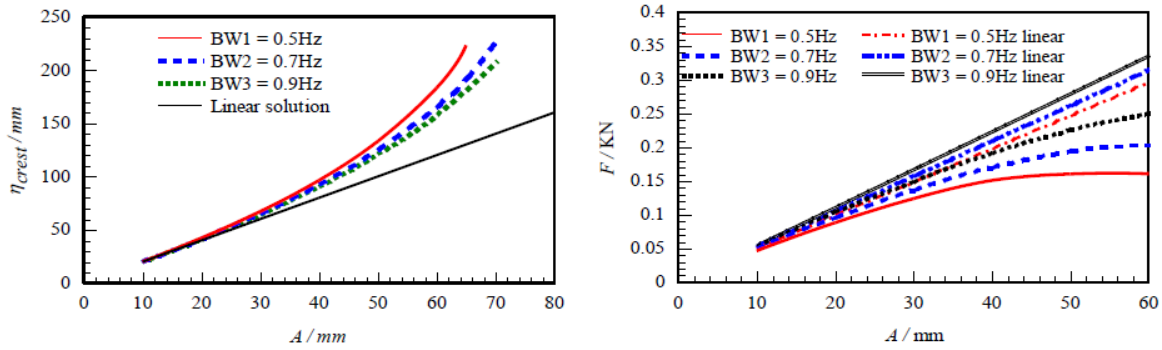

(a) the maximum crest elevation (b) the maximum wave loading

Fig.17. Variations of the maximum crest wave elevation and the maximum wave loading on the vertical seawall with input linear wave amplitude.

590